Energy storage in lead-free Ba(Zr, Ti)O_3 relaxor ferroelectrics: Large densities and efficiencies and their origins

Zhijun Jiang,[1,2] Sergey Prosandeev,[2] and L. Bellaiche[2]

[1]*MOE Key Laboratory for Nonequilibrium Synthesis and Modulation of Condensed Matter, Shaanxi Province Key Laboratory of Advanced Functional Materials and Mesoscopic Physics, School of Physics, Xi'an Jiaotong University, Xi'an 710049, China*

[2]*Physics Department and Institute for Nanoscience and Engineering, University of Arkansas, Fayetteville, Arkansas 72701, USA*

(Received 9 November 2021; accepted 8 December 2021; published 4 January 2022)

An atomistic first-principles-based effective Hamiltonian is used to investigate energy storage in $Ba(Zr_{0.5}Ti_{0.5})O_3$ relaxor ferroelectrics, both in their bulk and epitaxial films' forms, for electric fields applied along different crystallographic directions. We find that the energy density linearly increases with temperature for electric fields applied along the pseudocubic [001], [110], and [111] directions in $Ba(Zr_{0.5}Ti_{0.5})O_3$ bulk. For films at room temperature, the energy density adopts different behaviors (i.e., increase versus decrease) with strain depending on the direction of the applied electric fields. We also predicted ultrahigh energy densities (basically larger than 100 J/cm^3) with an ideal efficiency of 100% in all these $Ba(Zr_{0.5}Ti_{0.5})O_3$ systems. In addition, a phenomenological model is used to reveal the origin of all the aforementioned features, and should be applicable to other relaxor ferroelectrics.

DOI: 10.1103/PhysRevB.105.024102

I. INTRODUCTION

Dielectric capacitors are particularly promising for high-power energy storage applications because of their ultrafast charging/discharging rates and high reliability [1–7]. However, dielectric capacitors have relatively low energy densities and efficiencies, which is the main bottleneck towards applications in electronics and electric power systems. Intensive efforts have been devoted to find novel materials with higher energy density and efficiency. Recently, a special class of ferroelectrics with a frequency-dependent dielectric response-versus-temperature and several characteristic temperatures [8–12], namely the relaxor ferroelectrics, has been attracting much attention because of its ultrahigh energy densities and efficiencies [13–15]. One can for instance cite $Ba(Zr_xTi_{1-x})O_3$ thin films with a recoverable energy density of 156 J/cm^3 and an efficiency of 72.8% [13], $0.68Pb(Mg_{1/3}Nb_{2/3})O_3$-$0.32PbTiO_3$ (PMN-PT) films with 133 J/cm^3 and 75% [14], and Sm-doped yBFO-$(1-y)$BTO (Sm-BFBT) with 152 J/cm^3 and a marked enhancement of efficiency above 90% at an electric field of 3.5 MV/cm [15]. It is also worth noting that relaxor ferroelectrics in the range between the Burns temperature T_b and temperature T_m at which the dielectric constant exhibits a peak can be defined as superparaelectric relaxor ferroelectrics [15,16], which is highly promising for energy storage applications. As a matter of fact, the superparaelectric state in relaxor ferroelectrics can exhibit large polarizability at high electric fields with nonlinear *P-E* loop behavior while maintaining very small hysteresis [17].

Despite these impressive progresses on the use of relaxor ferroelectrics for energy storage, several questions remain unaddressed, to the best of our knowledge. For instance, can *ab initio based methods* reproduce the experimental finding about ultrahigh energy density in the lead-free relaxor $Ba(Zr_xTi_{1-x})O_3$ system, and, if yes, can they provide new insight into its origin? The effect of the direction of the applied electric field on energy storage density and efficiency is also presently unknown in this material, to the best of our knowledge. Similarly, we are not aware that the consequence of the epitaxial strain on energy-storage-related properties has ever been investigated, and thus revealed and explained, in films made of $Ba(Zr_xTi_{1-x})O_3$.

The aim of this paper is to answer all these questions, by using an atomistic first-principles-based effective Hamiltonian and analyzing its results via a simple and straightforward phenomenological model. In particular, we demonstrate, and explain why, ultrahigh energy density and efficiency can be achieved in $Ba(Zr_{0.5}Ti_{0.5})O_3$ ferroelectric relaxors, both in their bulk and epitaxial films' forms. The effects of the direction of the applied field as well as epitaxial strain are also revealed and understood.

This paper is organized as follows. Section II provides details about the atomistic effective Hamiltonian method used here. Sections III A and III B report and explain energy storage results in $Ba(Zr_{0.5}Ti_{0.5})O_3$ bulk and films, respectively. Finally, Sec. IV concludes this work.

II. METHODS

Here, the first-principles-based effective Hamiltonian (H_{eff}) approach that has been developed and used in Refs. [11,18–20] is employed to investigate bulk and epitaxial films made of $Ba(Zr_{0.5}Ti_{0.5})O_3$ (BZT) solid solutions. This H_{eff} successfully reproduced (i) the existence of tem-

peratures characteristic of relaxor ferroelectrics [11] (such as the Burns temperature T_b that typically marks the existence of dynamical polar nanoregions (PNRs) [11,21], $T_b \simeq 450$ K, the so-called T^* temperature at which static PNRs typically appear [11,22,23], $T^* \simeq 240$ K, and $T_m \simeq 130$ K, at which the dielectric response adopts a peak [8,11]); (ii) polar nanoregions [11,18]; and (iii) the unusual dielectric relaxation [24]—which is consistent with experimental findings for $Ba(Zr_xTi_{1-x})O_3$ system [25]. The total internal energy E_{int} of the H_{eff} consists of two main terms: $E_{int}(\{\mathbf{u}_i\}, \{\mathbf{v}_i\}, \eta_H, \{\sigma_j\}) = E_{ave}(\{\mathbf{u}_i\}, \{\mathbf{v}_i\}, \eta_H) + E_{loc}(\{\mathbf{u}_i\}, \{\mathbf{v}_i\}, \{\sigma_j\})$, where $\{\mathbf{u}_i\}$ is the local soft mode in unit cell i (which is proportional to the local electric dipole moment centered on Zr or Ti atoms), $\{\mathbf{v}_i\}$ are Ba-centered local displacements related to the inhomogeneous strain inside each cell, η_H represents the homogeneous strain tensor, and $\{\sigma_j\}$ characterizes the B sublattice atomic configuration in the BZT solid solutions. Actually, $\sigma_j = +1$ or -1 corresponds to the distribution of the Zr or Ti ion located at the j site of the B sublattice, respectively. The first energetic term of E_{ave} is composed of five energetic parts: (i) the local soft mode self-energy; (ii) the long-range dipole-dipole interaction; (iii) the short-range interactions between local soft modes; (iv) the elastic energy; and (v) the interaction between the local soft modes and strains [26]. The second term, E_{loc}, represents how the distribution of B sites (Zr and Ti ions) affects the energetics involving the local soft modes $\mathbf{u}_i$ and the local strain variables, which depends on the $\{\sigma_j\}$ atomic configuration distribution [11,18]. In order to mimic the effect under an applied dc electric field, an energy given by minus the dot product between polarization and applied electric field needs to be added to E_{int}. Note that we numerically find that the simulated electric field is larger than the corresponding experimental one by a factor of 100 in BZT when comparing the calculated polarization P with the experimental one for a $Ba(Zr_{0.5}Ti_{0.5})O_3$ thin film at room temperature [13]. Such discrepancy is typical for atomistic effective Hamiltonian simulations [27,28] and direct density functional theory (DFT) calculations [29–32], and is likely due to the fact that structural defects are not considered in these simulations. To address such discrepancy, we presently divide our theoretical field by a factor of 100 in the results to be reported and discussed below. Note also that we chose here a (renormalized) maximum applied electric field of $E_{max} = 3.0 \times 10^8$ V/m, which has been experimentally achieved in $Ba(Zr_xTi_{1-x})O_3$ thin films [13].

Moreover, we employ the effective Hamiltonian scheme within Monte Carlo (MC) simulations on $12 \times 12 \times 12$ supercells (8640 atoms) with periodic boundary conditions and the distribution of Zr and Ti ions is chosen randomly over the B sublattice. In the case of the films grown along the [001] pseudocubic direction, epitaxial strains are associated with the freezing of some components of the homogeneous strain tensors, namely (in Voigt notation) $\eta_6 = 0$ and $\eta_1 = \eta_2 = (a_{sub} - a_{eq})/a_{eq}$, where a_{sub} and a_{eq} are the lattice constants of the substrate and BZT bulk at 130 K, respectively [19]. We also limited the simulations for strains ranging between -3% and $+3\%$, which is a physically reasonable range. Note that the films are periodic along the three Cartesian directions and only the strain is thus considered here when modeling epitaxial films (i.e., no surface or thickness effects are taken into account).

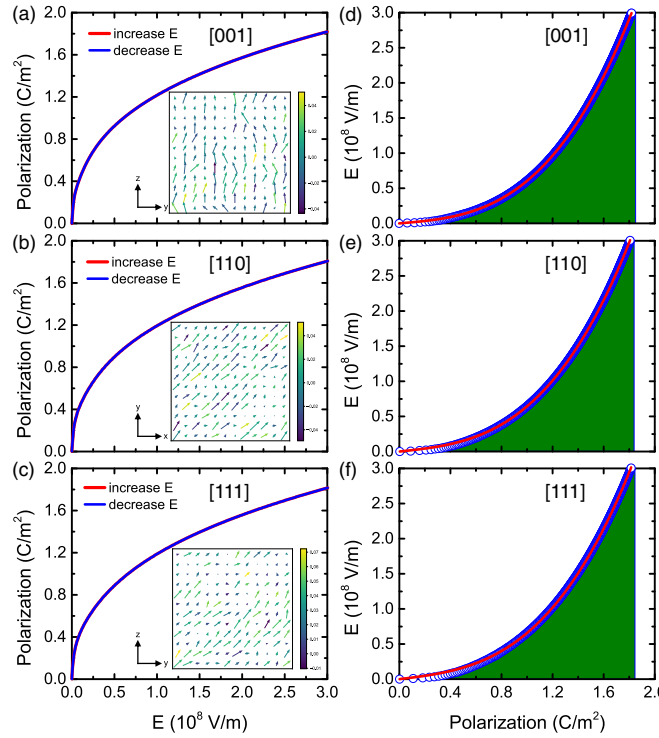

FIG. 1. (a)–(c) P-E hysteresis curves at 300 K for electric fields applied along the pseudocubic [001], [110], and [111] directions, respectively, in BZT bulk. The insets show the dipolar configurations in a given (y, z) or (x, y) plane at 300 K for the magnitude of the field equal to $\simeq 0.1 \times 10^8$ V/m with three different field's applied directions. (d)–(f) Electric field versus polarization at 300 K for electric fields applied along the pseudocubic [001], [110], and [111] directions, respectively. The green areas represent the energy densities and the solid red lines represent the fit of the MC data by the Landau model.

III. RESULTS AND DISCUSSION

A. Energy storage in BZT bulk

Figures 1(a)–1(c) show the P-E curves at a selected room temperature of 300 K for electric fields applied along the pseudocubic [001], [110], and [111] directions, respectively, in BZT bulk. For all these directions, the resulting polarization aligns along the field. As depicted in Figs. 1(a)–1(c), the charging and discharging processes of the P-E curves are completely reversible, which implies that the energy efficiency is 100% (the charging and discharging cycles correspond to electric field increasing from zero to $E_{max} = 3.0 \times 10^8$ V/m and then decreasing back to zero field, respectively). Note that the ideal 100% efficiency has also been predicted in epitaxial AlN/ScN superlattices [32] as a result of a field-induced *second-order* transition towards a ferroelectric state. In the case of BZT, measurements also found a large value for this efficiency, namely of $82.4 \pm 1.0\%$ at an electric field $\simeq 3.0 \times 10^8$ V/m [13] (the deviation from the ideal value of

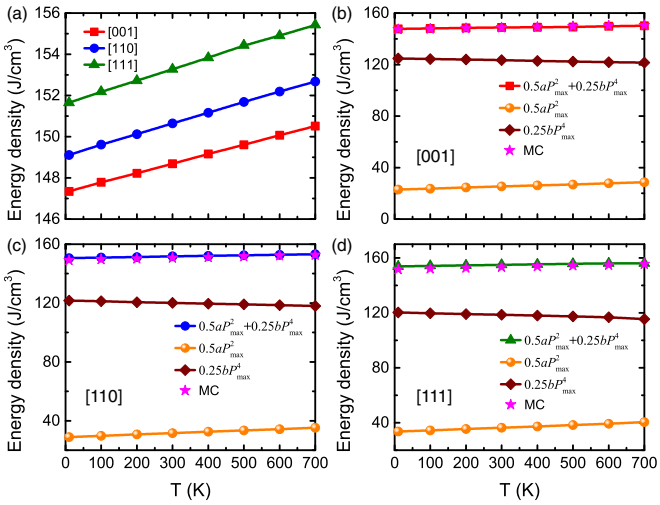

FIG. 2. (a) Energy density obtained from MC data as a function of temperature for electric fields applied along the [001], [110], and [111] directions, with a maximal electric field being equal to 3.0×10^8 V/m, in BZT bulk. (b)–(d) Total and decomposed energy densities obtained from Eq. (3) as a function of temperature at $E_{max} = 3.0 \times 10^8$ V/m for electric fields applied along the [001], [110], and [111] directions, respectively. Stars also display the MC data of the total energy densities again in (b)–(d) for comparison.

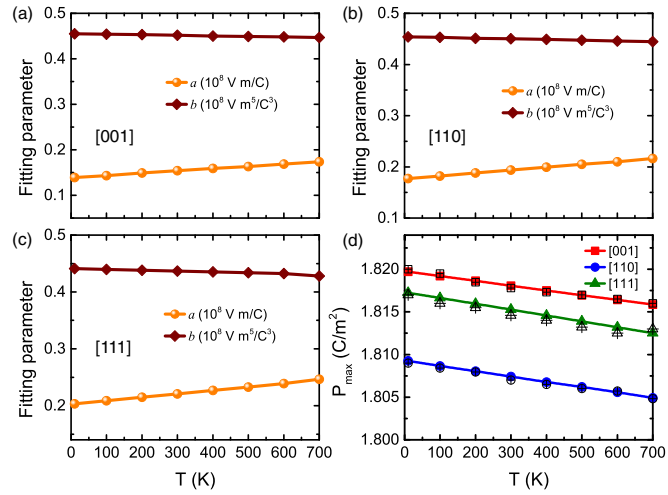

FIG. 3. (a)–(c) Temperature dependence of fitting parameters a and b (see text) for electric fields applied along the [001], [110], and [111] directions, respectively, with a maximal applied electric field of $E_{max} = 3.0 \times 10^8$ V/m, in BZT bulk. (d) P_{max} obtained from MC data (filled symbols) and Eq. (2) (open symbols) as a function of temperature at $E_{max} = 3.0 \times 10^8$ V/m for electric fields applied along the [001], [110], and [111] directions, in BZT bulk.

100% may also arise from the presence of defects in the grown sample).

Moreover, the insets of Figs. 1(a)–1(c) display the local dipole configurations in a given (y, z) or (x, y) plane at 300 K for these three different applied field directions with a magnitude of $\simeq 0.1 \times 10^8$ V/m. Recalling that the H_{eff} predicted that, under zero field and for temperatures below the Burns temperature ($T_b \simeq 450$ K) [11], BZT possesses different polar nanoregions for which the dipoles align along different ⟨111⟩ pseudocubic directions (hence resulting in an overall vanishing polarization), these insets demonstrate that the application of electric field along a given direction forces dipoles to rotate towards the field's direction (hence giving rise to a finite polarization along that latter direction).

Furthermore, Figs. 1(d)–1(f) display the electric field applied along these [001], [110], and [111] pseudocubic directions as a function of polarization for temperature at 300 K, which allows us to extract the energy density since it is simply the green area shown in these figures.

Doing that for all considered temperatures (up to 700 K) therefore allows us to compute the energy densities as a function of temperature for electric fields applied along the [001], [110], and [111] pseudocubic directions, which are shown in Fig. 2(a). It is interesting to realize that (1) the energy densities linearly increase with temperature for the three different considered field's directions; and (2) we predict ultrahigh energy densities and values varying between 147 and 155 J/cm^3, which agrees very well with experimental reports in $Ba(Zr_xTi_{1-x})O_3$ thin films [13].

In order to understand the origin of these energy density features, let us take advantage of the simple Landau-type free energy model developed in Ref. [32]:

$$F = \tfrac{1}{2}aP^2 + \tfrac{1}{4}bP^4 - EP, \qquad (1)$$

where a and b are quadratic and quartic coefficients, respectively.

At equilibrium, one must have $\frac{\partial F}{\partial P} = 0$, which thus leads to

$$E = aP + bP^3. \qquad (2)$$

Interestingly, the electric field versus polarization (E-P) MC data for all considered temperatures can indeed be nicely fitted by Eq. (2), which shows that such equation is valid but also allows us to extract the a and b parameters for each temperature and considered field's direction. These latter a and b coefficients are shown in Figs. 3(a)–3(c) as a function of temperature for fields up to the maximum field $E_{max} = 3.0 \times 10^8$ V/m applied along the [001], [110], and [111] pseudocubic directions, respectively. These a and b coefficients are important for energy storage since they are involved in the expression of the energy density, according to the Landau model [32]:

$$U = \int_0^{P_{max}} (aP + bP^3)dP = \frac{1}{2}aP_{max}^2 + \frac{1}{4}bP_{max}^4, \qquad (3)$$

where P_{max} is the polarization at E_{max}. Note that, practically, one can determine P_{max} via two different ways, that are directly from the MC data or via Eq. (2) at the field of E_{max} since a and b parameters are now known. As shown in Fig. 3(d), these two methods give nearly identical results.

Equation (3) therefore tells us that only three quantities completely govern the behaviors and values of the energy density, namely a, b, and P_{max}. It is thus necessary to comment on their behaviors with temperature and field's direction that are reported in Fig. 3. The fitting parameter a linearly increases with temperature for the three different field's directions—as expected from usual Landau theory of ferroelectrics stating that this coefficient should be equal to $a_0(T - T_c)$, where a_0 is a positive constant and T_c is a critical

temperature (that can be negative for relaxor ferroelectrics) [33]. It varies from 0.139×10^8 to 0.174×10^8 V m/C for the [001] direction, from 0.177×10^8 to 0.216×10^8 V m/C for [110], and from 0.203×10^8 to 0.247×10^8 V m/C for [111], respectively, for temperatures ranging between 10 and 700 K. In contrast, the b parameter only slightly linearly decreases with temperature (its value concomitantly ranges from 0.455×10^8 to 0.447×10^8 V m^5/C^3 for [001], from 0.454×10^8 to 0.445×10^8 V m^5/C^3 for [110], and from 0.441×10^8 to 0.428×10^8 V m^5/C^3 for [111], respectively). Finally, $P_{\max}$ basically only very slightly linearly decreases with temperature from 1.820 to 1.816 C/m^2 for fields applied along [001], from 1.809 to 1.805 C/m^2 for [110], and from 1.817 to 1.813 C/m^2 for [111], respectively, with temperatures varying from 10 to 700 K. Its rather large value indicates that BZT is easily polarizable. The parameter that is the most sensitive to both temperature and field's direction is therefore the a coefficient. Its temperature behavior (linear increase and always positive values) basically indicates that increasing the temperature makes BZT go further away from a ferroelectric state at zero field for any direction of the field. Its dependency on field's direction at any temperature (smaller positive values a for the [001] direction and larger values for [111]) reveals that it is easier to induce a ferroelectric state when applying an electric field along [001] than [110] and then [111]—likely because inducing a ferroelectric state with a polarization along [111] requires the polar nanoregions existing at zero field and having electric dipoles along $[\bar{1}\bar{1}\bar{1}]$ to completely revert their polarization rather than simply rotate towards an intermediate direction, such as [001].

The behaviors of a, b, and $P_{\max}$ allow us to understand the results of the energy density in Fig. 2(a) since Eq. (3) indicates that such energy density can be decomposed into two terms, that are $\frac{1}{2}aP_{\max}^2$ and $\frac{1}{4}bP_{\max}^4$, and which are shown in Figs. 2(b)–2(d) for the three different field's directions with $E_{\max} = 3.0 \times 10^8$ V/m, along with the (total) energy densities directly obtained from the MC data. One can clearly see that, for any considered temperature, Eq. (3) and the MC energy densities provide nearly identical results. Since b and $P_{\max}$ are in first approximation independent of both the temperature and the field's direction, the dependencies of the total energy density on temperature and crystallographic direction of the electric field basically arise from the aforementioned corresponding dependencies of the a parameter. Note that the contribution of $\frac{1}{2}aP_{\max}^2$ ($\frac{1}{4}bP_{\max}^4$) to the total energy density at 300 K is 17% (83%), 21% (79%), and 23% (77%) for electric fields applied along the [001], [110], and [111] directions, respectively. These numbers, as well as Figs. 2 and 3 and Eq. (3), therefore tell us that having a large energy density accompanied by a large efficiency can be accomplished by (1) having large positive a and b coefficients, which characterize systems that cannot be energetically too close to a ferroelectric state and that will undergo a second-order field-induced transition to a ferroelectric state at large fields; while (2) having a large $P_{\max}$ at feasible electric fields, which indicates that the system is easily polarizable at these fields and which thus also implies that a and b cannot be too large. Note that conditions (1) and (2) are relevant to analyze and understand the ultrahigh energy storage in initially nonpolar AlN/ScN superlattices [32] and superparaelectric relaxor ferroelectrics [15].

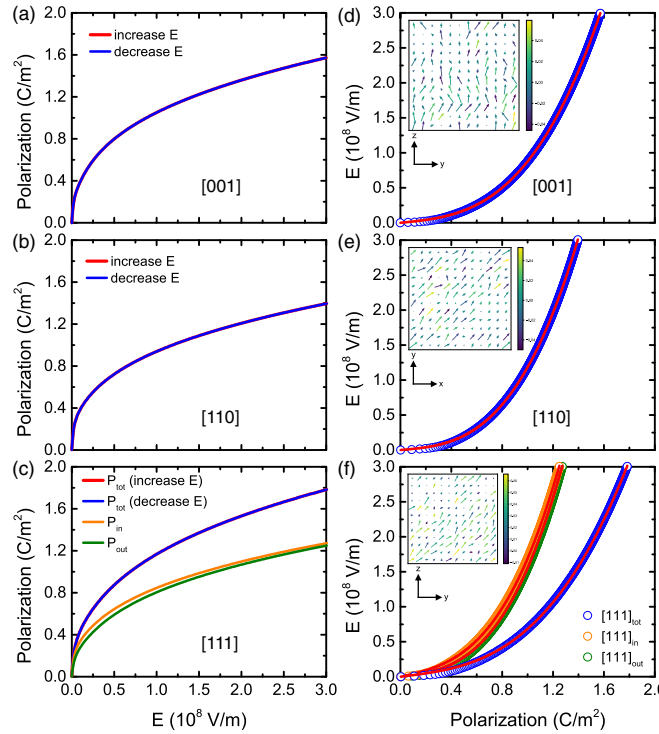

FIG. 4. Same as Fig. 1 but for (001) BZT films at 0% strain.

B. Energy storage in (001) BZT films

Let us now present the energy storage results for (001) BZT films as a function of epitaxial strain for the selected temperature of 300 K. Figures 4(a)–4(c) respectively show the P-E curves at 300 K and zero strain for fields applied along (i) the pseudocubic [001] that results in a polarization lying along that out-of-plane direction; (ii) the [110] direction that yields a polarization aligned along that in-plane direction; and (iii) the [111] direction that induces a polarization being along $[uuv]$ direction, that is $P_x = P_y \neq P_z$, due to the freezing of $\eta_1 = \eta_2$ strain components while η_3 can relax. Note that the direction of these polarization in the three cases is also consistent with the insets of Figs. 4(d)–4(f) showing the dipole configurations in a given (y, z) or (x, y) plane at zero strain and 300 K. Note also that, consequently, we show three types of P-E data for fields applied along the [111] direction in Fig. 4(c), that is for the in-plane component of the polarization P_{in} (which is along the [110] direction), the out-of-plane component of the polarization P_{out} (that is along [001]) and the total polarization P_{tot} (that is given by $P_{\text{tot}} = \sqrt{P_x^2 + P_y^2 + P_z^2}$).

Moreover, Figs. 4(d)–4(f) show the corresponding E-P data at zero strain and 300 K for fields applied along these three different directions up to $E_{\max} = 3.0 \times 10^8$ V/m, which, once again, allows the energy density to be extracted via the computation of areas similar to the green ones of Figs. 1(d)–1(f). Such types of calculations are then performed for all considered strains at 300 K, which yields the results for energy density reported in Fig. 5 for the different directions of the field. Note that we continue to distinguish between in-plane

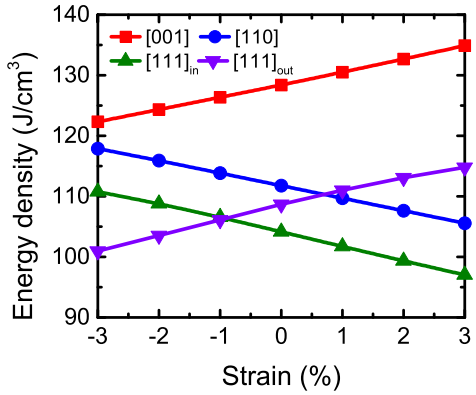

FIG. 5. Energy density obtained from MC data versus strain at 300 K and $E_{max} = 3.0 \times 10^8$ V/m for fields applied along the [001], [110], and [111] directions, respectively, in (001) BZT films. The distinction between $[111]_{in}$ versus $[111]_{out}$ is explained in the text, in case of fields applied along [111].

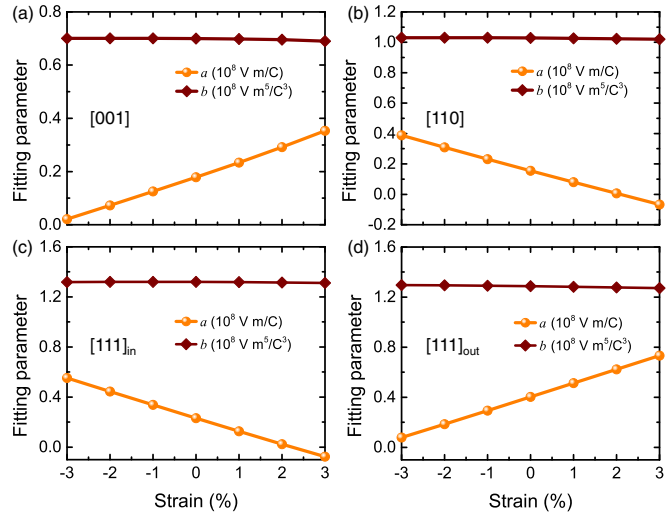

FIG. 6. (a),(b) Same as Figs. 3(a) and 3(b) but as a function of strain at 300 K in BZT films. Panels (c) and (d) show the in-plane and out-of-plane fitting parameters a and b when field is applied along the [111] direction, respectively.

versus out-of-plane components of the polarization in case of a field applied along [111], with this distinction resulting in the wording of $[111]_{in}$ versus $[111]_{out}$ in Figs. 4(f) and 5 as well as in the text.

One can first realize that for all considered strains, the energy density is still large in magnitude in the films (typically larger than 100 J/cm^3), while being smaller than that of BZT bulk at room temperature. For instance, the energy densities of bulk BZT at 300 K are 148.7 J/cm^3 when the field is applied along [001], 150.6 J/cm^3 for [110], and 153.3 J/cm^3 for [111], respectively. This slight decrease when going from bulk to films originates from the fact that, for each considered field and at a fixed temperature, the in-plane lattice constants are constant in the epitaxial films while they can vary when changing the fields in the bulk—which can thus give rise to larger polarizations in bulk than in films. Other striking features of Fig. 5 are that the energy densities resulting from the application of a field along [001] as well as the one associated with the out-of-plane component of polarization under a [111] field, that is $[111]_{out}$, both linearly increase with strain ranging between -3% and $+3\%$. In contrast, the energy densities when the field is applied along [110] and the other one linked with in-plane component of polarization, namely $[111]_{in}$, both linearly decrease with such strain. Furthermore, the largest energy density is found for our maximal considered tensile strain (that is $+3\%$) in case of a field applied along [001].

To understand the energy density results in Fig. 5 for (001) BZT films, we also decided to use Eq. (2) (which is once again found to fit well the MC data) and Eq. (3). Consequently, Fig. 6 shows the a and b fitting parameters while Fig. 7 displays the resulting P_{max}, for these films. Figures 6(a) and 7 indicate that, when the field is applied along the [001] direction, the (i) fitting parameter a is positive and linearly increases when the strain increases from -3% to $+3\%$ (a varies from 0.02×10^8 to 0.35×10^8 V m/C); (ii) b coefficient is basically a constant with strain (it varies from 0.70×10^8 to 0.69×10^8 V m^5/C^3); and (iii) P_{max} linearly decreases with strain from 1.62 to 1.53 C/m^2. In contrast, when the field is along [110], Figs. 6(b) and 7 reveal that (iv) a linearly decreases with strain (from 0.39×10^8 to -0.07×10^8 V m/C, therefore becoming slightly negative at large tensile strains); (v) P_{max} linearly increases with strain (from 1.34 to 1.45 C/m^2); (vi) while b continues to be basically constant with strain (it only changes from 1.03×10^8 to 1.02×10^8 V m^5/C^3). Items (i)–(vi) can be simply understood by realizing that increasing strain from compressive to tensile in epitaxial (001) films is known to progressively disfavor a ferroelectric state with an out-of-plane polarization in favor of a ferroelectric state with an in-plane polarization [34–36]. For the same reasons and as shown in Figs. 6(c), 6(d), and 7, the a parameter and P_{max} associated with the out-of-plane (respectively, in-plane) components for fields applied along [111] have the same behavior with strain as those for the field lying along [001] (respectively, [110]). Note also that the b parameter continues to be basically independent of strain in the case of fields applied [111], as well—which reveals that BZT can adopt *second-order* phase transition when under strain and/or field [18].

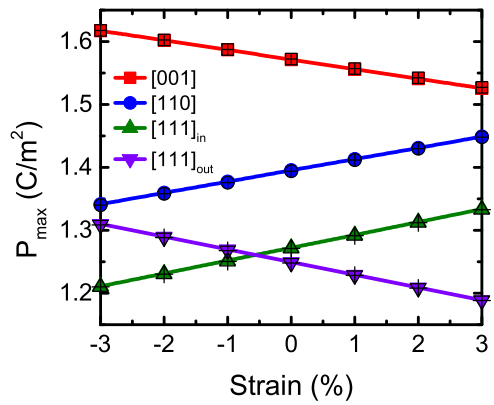

FIG. 7. Same as Fig. 3(d) but as a function of strain at 300 K in BZT films.

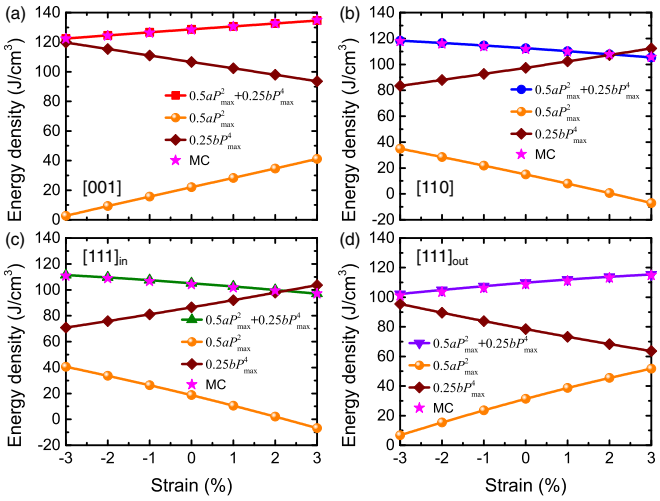

FIG. 8. (a)–(d) Total and decomposed energy densities versus strain for fields applied along [001] (a), [110] (b), and [111] (c),(d) for in-plane versus out-of-plane components of the polarization, at a maximal applied electric field equal to 3.0×10^8 V/m and 300 K in BZT films.

Let us now pay attention to the two terms of Eq. (3) that sum up to be the total energy density. They are shown in Fig. 8, using the fitting parameters (a and b) of Fig. 6 and P_{max} of Fig. 7. Due to the aforementioned behavior of a that grows faster than P_{max} decreases with strain, the first contribution, $\frac{1}{2}aP^2_{max}$, increases with strain (from 2.7 for -3% to 41.1 J/cm^3 for $+3\%$), when the field is applied along the [001] direction, as displayed in Fig. 8(a). In contrast, the second contribution, $\frac{1}{4}bP^4_{max}$, decreases with strain from 119.8 to 93.6 J/cm^3 when the field is also along this [001] direction, as a result of the concomitant decrease of P_{max} while b is basically constant with strain. Note that the change of value in $\frac{1}{4}bP^4_{max}$ is smaller than $\frac{1}{2}aP^2_{max}$ for this field's direction, once again because of the fast increase of a with strain reflecting the desire of the system to be energetically far from a polarized state with a polarization along [001] when enhancing the strain from compressive to tensile values. Consequently, the total energy density increases with strain.

The behaviors are opposite when the field is applied along [110] because BZT films become much closer in energy to adopt a ferroelectric state with an in-plane [110] polarization direction as the strain is enhanced. Consequently, a strongly decreases with strain while P_{max} is enhanced but at a smaller extent. As a result, $\frac{1}{2}aP^2_{max}$ decreases with strain (values varying between 34.9 and -7.1 J/cm^3) faster than $\frac{1}{4}bP^4_{max}$ increases (from 83.5 to 112.4 J/cm^3) for fields applied along the [110] direction—as shown in Fig. 8(b). The resulting total energy density thus decreases with strain.

Regarding the energy density for fields applied along the [111] direction, Fig. 8(c) [respectively, Fig. 8(d)] that is related to the in-plane (respectively, out-of-plane) component of the polarization shows that the behaviors of total and decomposed energy densities are very similar to Fig. 8(b) that corresponds the field applied along [110] [respectively to Fig. 8(a) that corresponds the field applied along [001]] for the same energetic reasons, i.e., going from compressive strain to tensile strain favors the formation of in-plane polarization while disfavoring ferroelectric states with out-of-plane polarization.

IV. SUMMARY

In summary, an atomistic effective Hamiltonian scheme combined with Monte Carlo simulations was used to investigate the energy storage in bulk and epitaxial (001) films made of BZT. We find that these BZT systems can exhibit ultrahigh energy densities and an ideal efficiency of 100%. These energy storage results are then interpreted via a simple phenomenological model that reproduces these MC data. More precisely, energy density can be decomposed into two terms: the first term being the product of the fitting a parameter and P^2_{max}, and the second term being the product between the b parameter and P^4_{max}. The behavior of a, b, and P_{max} lead to a competition between these two terms (that can be understood in terms of energetics) that eventually causes the temperature dependency, field's direction dependency, and strain dependency of the total energy density. The proposed phenomenological model can be easily employed for nonlinear dielectrics with large energy density. We thus hope that the present paper deepens the fields of energy storage in relaxor ferroelectrics and other nonlinear dielectrics.

ACKNOWLEDGMENTS

This work was supported by the National Natural Science Foundation of China (Grant No. 11804138), Shandong Provincial Natural Science Foundation (Grant No. ZR2019QA008), China Postdoctoral Science Foundation (Grants No. 2020T130120 and No. 2018M641905), and "Young Talent Support Plan" of Xi'an Jiaotong University (Grant No. WL6J004). S.P and L.B. acknowledge the Office of Naval Research for the support under Grants No. N00014-17-1-2818 and No. N00014-21-1-2086. L.B. also acknowledges ARO Grant No. W911NF-21-1-0113 and the Vannevar Bush Faculty Fellowship Grant No. N00014-20-1-2834 from the Department of Defense. The Arkansas High Performance Computing Center (AHPCC) and the HPC Platform of Xi'an Jiaotong University are also acknowledged.

[1] B. Chu, X. Zhou, K. Ren, B. Neese, M. Lin, Q. Wang, F. Bauer, and Q. M. Zhang, Science **313**, 334 (2006).

[2] Q. Li, L. Chen, M. R. Gadinski, S. Zhang, G. Zhang, H. U. Li, E. Iagodkine, A. Haque, L.-Q. Chen, T. N. Jackson, and Q. Wang, Nature (London) **523**, 576 (2015).

[3] B. Peng, Q. Zhang, X. Li, T. Sun, H. Fan, S. Ke, M. Ye, Y. Wang, W. Lu, H. Niu, J. F. Scott, X. Zeng, and H. Huang, Adv. Electron. Mater. **1**, 1500052 (2015).

[4] Prateek, V. K. Thakur, and R. K. Gupta, Chem. Rev. **116**, 4260 (2016).

[5] H. Palneedi, M. Peddigari, G.-T. Hwang, D.-Y. Jeong, and J. Ryu, Adv. Funct. Mater. **28**, 1803665 (2018).
[6] L. Yang, X. Kong, F. Li, H. Hao, Z. Cheng, H. Liu, J.-F. Li, and S. Zhang, Prog. Mater. Sci. **102**, 72 (2019).
[7] H. Pan, F. Li, Y. Liu, Q. Zhang, M. Wang, S. Lan, Y. Zheng, J. Ma, L. Gu, Y. Shen, P. Yu, S. Zhang, L.-Q. Chen, Y.-H. Lin, and C.-W. Nan, Science **365**, 578 (2019).
[8] L. E. Cross, Ferroelectrics **151**, 305 (1994).
[9] A. A. Bokov and Z.-G. Ye, J. Mater. Sci. **41**, 31 (2006).
[10] V. V. Shvartsman and D. C. Lupascu, J. Am. Ceram. Soc. **95**, 1 (2012).
[11] A. R. Akbarzadeh, S. Prosandeev, E. J. Walter, A. Al-Barakaty, and L. Bellaiche, Phys. Rev. Lett. **108**, 257601 (2012).
[12] A. Al-Barakaty, S. Prosandeev, D. Wang, B. Dkhil, and L. Bellaiche, Phys. Rev. B **91**, 214117 (2015).
[13] A. A. Instan, S. P. Pavunny, M. K. Bhattarai, and R. S. Katiyar, Appl. Phys. Lett. **111**, 142903 (2017).
[14] J. Kim, S. Saremi, M. Acharya, G. Velarde, E. Parsonnet, P. Donahue, A. Qualls, D. Garcia, and L. W. Martin, Science **369**, 81 (2020).
[15] H. Pan, S. Lan, S. Xu, Q. Zhang, H. Yao, Y. Liu, F. Meng, E.-J. Guo, L. Gu, D. Yi, X. R. Wang, H. Huang, J. L. MacManus-Driscoll, L.-Q. Chen, K.-J. Jin, C.-W. Nan, and Y.-H. Lin, Science **374**, 100 (2021).
[16] L. E. Cross, Ferroelectrics **76**, 241 (1987).
[17] A. E. Glazounov, A. J. Bell, and A. K. Tagantsev, J. Phys.: Condens. Matter **7**, 4145 (1995).
[18] S. Prosandeev, D. Wang, A. R. Akbarzadeh, B. Dkhil, and L. Bellaiche, Phys. Rev. Lett. **110**, 207601 (2013).
[19] S. Prosandeev, D. Wang, and L. Bellaiche, Phys. Rev. Lett. **111**, 247602 (2013).
[20] Z. Jiang, S. Prokhorenko, S. Prosandeev, Y. Nahas, D. Wang, J. Íñiguez, E. Defay, and L. Bellaiche, Phys. Rev. B **96**, 014114 (2017).
[21] G. Burns and F. H. Dacol, Phys. Rev. B **28**, 2527 (1983).
[22] B. Dkhil, P. Gemeiner, A. Al-Barakaty, L. Bellaiche, E. Dul'kin, E. Mojaev, and M. Roth, Phys. Rev. B **80**, 064103 (2009).
[23] O. Svitelskiy, D. La-Orauttapong, J. Toulouse, W. Chen, and Z.-G. Ye, Phys. Rev. B **72**, 172106 (2005).
[24] D. Wang, A. A. Bokov, Z.-G. Ye, J. Hlinka, and L. Bellaiche, Nat. Commun. **7**, 11014 (2016).
[25] T. Maiti, R. Guo, and A. S. Bhalla, J. Am. Ceram. Soc. **91**, 1769 (2008).
[26] W. Zhong, D. Vanderbilt, and K. M. Rabe, Phys. Rev. B **52**, 6301 (1995).
[27] B. Xu, J. Íñiguez, and L. Bellaiche, Nat. Commun. **8**, 15682 (2017).
[28] Z. Jiang, Y. Nahas, S. Prokhorenko, S. Prosandeev, D. Wang, J. Íñiguez, and L. Bellaiche, Phys. Rev. B **97**, 104110 (2018).
[29] J. Lu, G. Chen, W. Luo, J. Íñiguez, L. Bellaiche, and H. Xiang, Phys. Rev. Lett. **122**, 227601 (2019).
[30] L. Chen, C. Xu, H. Tian, H. Xiang, J. Íñiguez, Y. Yang, and L. Bellaiche, Phys. Rev. Lett. **122**, 247701 (2019).
[31] Z. Jiang, C. Paillard, H. Xiang, and L. Bellaiche, Phys. Rev. Lett. **125**, 017401 (2020).
[32] Z. Jiang, B. Xu, H. Xiang, and L. Bellaiche, Phys. Rev. Mater. **5**, L072401 (2021).
[33] P. Chandra and P. B. Littlewood, A Landau Primer for Ferroelectrics, in *Physics of Ferroelectrics: A Modern Perspective*, edited by K. M. Rabe, C. H. Ahn, and J.-M. Triscone (Springer, Berlin, 2007), pp. 69–116.
[34] B. Dupé, S. Prosandeev, G. Geneste, B. Dkhil, and L. Bellaiche, Phys. Rev. Lett. **106**, 237601 (2011).
[35] Y. Yang, W. Ren, M. Stengel, X. H. Yan, and L. Bellaiche, Phys. Rev. Lett. **109**, 057602 (2012).
[36] L. Chen, Y. Yang, Z. Gui, D. Sando, M. Bibes, X. K. Meng, and L. Bellaiche, Phys. Rev. Lett. **115**, 267602 (2015).